

## Full exploitation of the HYMAGYC code for a shaped cross section scenario

G. Fogaccia, G. Vlad, S. Briguglio and V. Fusco

ENEA, Fusion and Nuclear Safety Department, C. R. Frascati, via E. Fermi 45, I-00044  
Frascati (Roma), Italy

One of the major challenges in magnetic confinement thermonuclear fusion research concerns the confinement, inside the reaction chamber of a burning plasma, of the energetic particles (EPs) produced by fusion reactions and/or by additional heating systems as electron and ion cyclotron resonant heating and neutral beam injection. Energetic particles in such experiments have velocities of the order of the Alfvén velocity, and then, they can resonantly interact with the shear Alfvén waves, driving global modes, which, in turn, could enhance the EP transport toward the first wall and lead to a significant particle and heat load. In order to predict and, eventually, minimize the EP transport in the next generation fusion devices, several numerical models, based on different theoretical approaches, have been developed. Here we present results obtained with the recently developed hybrid mhd-gyrokinetic code HYMAGYC [1], suited to study the interaction between EPs and Alfvénic modes in general high- $\beta$  axisymmetric equilibria, ( $\beta$  being the ratio of the plasma pressure to the magnetic one), with fully retained perturbed electromagnetic fields (electrostatic potential  $\varphi$  and vector potential  $\mathbf{A}$ ). The thermal plasma is described as a single fluid by full resistive linear MHD equations. The field solver originates from the code MARS [2], transformed from an eigenvalue solver to an initial value one. Energetic particles are described by nonlinear gyrokinetic Vlasov equations [3] solved by particle-in-cell (PIC) techniques and expanded up to order  $O(\epsilon^2)$  and  $O(\epsilon\epsilon_B)$ ,  $\epsilon$  being the gyrokinetic ordering parameter  $\epsilon \approx \rho_H/L_n$  and  $\epsilon_B \approx \rho_H/L_B$ , with  $\rho_H$  the EP (“Hot”) Larmor radius, and  $L_n$  and  $L_B$  the nonuniformity characteristic length scales of the equilibrium plasma density and magnetic field, respectively. The following space-time ordering for the fluctuating electromagnetic fields holds:  $k_\perp \rho_H = O(1)$ ,  $k_\parallel \rho_H = O(\epsilon)$ ,  $\omega/\Omega_H = O(\epsilon)$ , being  $k_\perp$  the perpendicular (to the equilibrium magnetic field) wave vector of perturbed fields,  $k_\parallel$  the parallel one,  $\omega$  the characteristic fluctuation frequency and  $\Omega_H$  the EP gyrofrequency. The two modules, the MHD and the gyrokinetic one, are coupled together by inserting the divergence of the EP pressure tensor in the MHD momentum equations [4]. In this work all the code capabilities have been fully exploited: a realistic shaped cross section equilibrium (we have considered a AUG model scenario [5]), finite magnetic compression ( $\delta A_\perp \neq 0$ ), Finite Larmor Radius (FLR) effects. The AUG model scenario has been identified in collaboration

with the NLED Enabling Research group [6] and analyzed by CHEASE [7] in order to compute the equilibrium quantities required by HYMAGYC (as, e.g., the metric tensor components, equilibrium magnetic field, current and pressure components). The AUG NLED

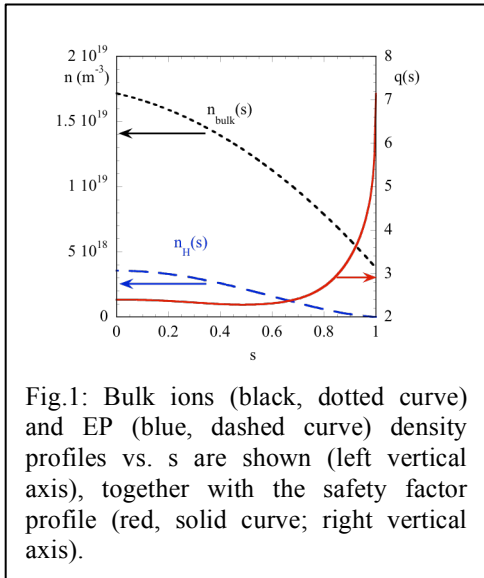


Fig.1: Bulk ions (black, dotted curve) and EP (blue, dashed curve) density profiles vs.  $s$  are shown (left vertical axis), together with the safety factor profile (red, solid curve; right vertical axis).

model equilibrium is characterized by on-axis magnetic field  $B_0=2.208\text{T}$ , magnetic axis radius  $R_0=1.666\text{m}$ , minor radius  $a=0.482\text{m}$  geometrical major radius of the torus  $R_{\text{geo}}=1.62\text{m}$  and a shaped poloidal cross section. The safety factor  $q$  profile along the flux-like radial coordinate  $s=(\psi_{\text{norm}})^{1/2}$  with  $\psi_{\text{norm}}$  the normalized poloidal flux, is shown in Fig.1. Using the MHD linear stability eigenvalue code MARS, the shear Alfvén continua for general toroidal mode numbers can be obtained: such continua will be used later on when discussing the

EP driven modes (see, e.g., Figs. 3,4). Finally, by introducing a Maxwellian EP population of deuterium characterized by a flat temperature  $T_H=0.093\text{ MeV}$  and a monotonic density profile

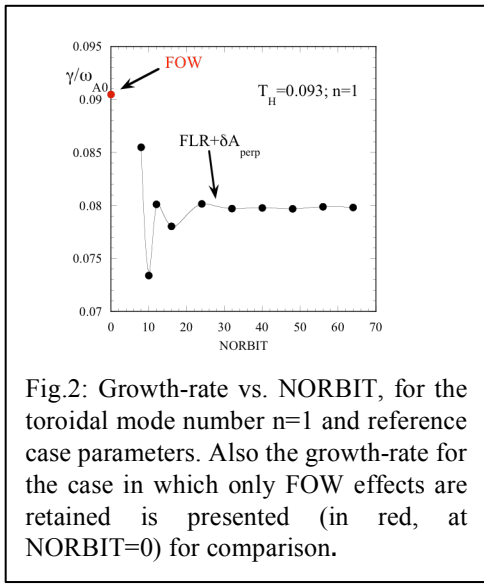


Fig.2: Growth-rate vs. NORBIT, for the toroidal mode number  $n=1$  and reference case parameters. Also the growth-rate for the case in which only FOW effects are retained is presented (in red, at NORBIT=0) for comparison.

(see Fig.1), unstable modes appear. Note that with the above mentioned parameters the ratio of on-axis EP thermal velocity to the on-axis Alfvén velocity is  $v_H/v_{A0} \approx 0.257$  and the ratio of the on-axis EP Larmor radius to the minor radius is  $\rho_H/a \approx 0.04$  with the EP thermal velocity being defined as  $v_H=(T_H/m_H)^{1/2}$ .

In the following we will present results both considering only Finite Orbit Width (FOW) effects as well as fully retaining FLR and magnetic compression effects. For the latter case, gyro-average

along the EP Larmor orbits is needed, in order to properly retain the FLR effects, thus requiring evaluating the contribution of each EP on several gyro-phase positions. In Fig.2 the dependence of the growth-rate on such number of positions is shown, for the reference case of the AUG equilibrium and  $n=1$ : the adequate number of points to compute the gyro average is in this case  $\text{NORBIT} \geq 32$  to retain correctly the FLR effects.

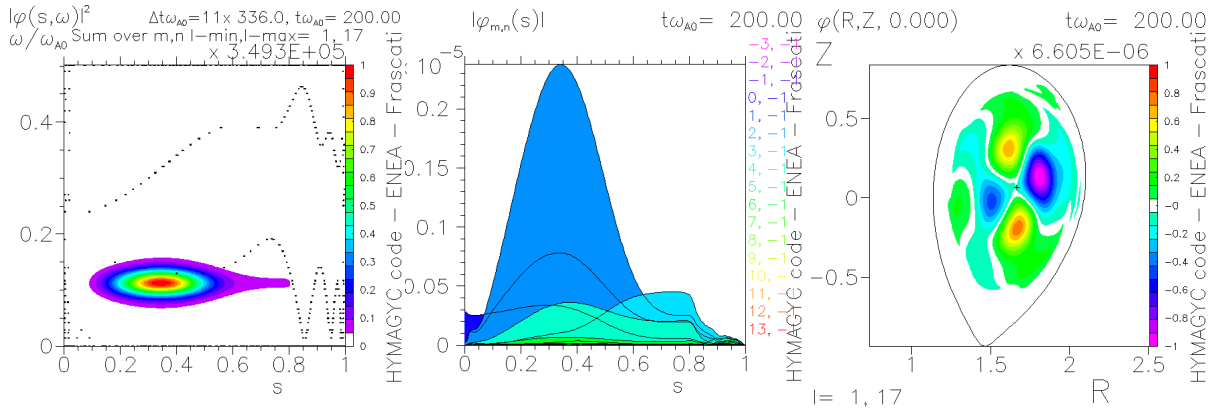


Fig.3. Toroidal mode number  $n=1$  retaining only FOW effects. Left: power spectrum of the fluctuating electrostatic potential  $\varphi$  in the plane  $(s, \omega)$ ; Alfvén continua are also shown with black dots. Center: poloidal Fourier components of the electrostatic potential  $|\varphi_{m,n=1}|$  vs.  $s$ . Right: electrostatic potential  $\varphi(R, Z)$  for the toroidal angle  $\phi=0$ .

In the following we will present the linear stability results for two values of the toroidal mode number  $n=1, 3$ ; for simplicity, simulations with the adiabatic index  $\Gamma=0$  have been considered ( $\Gamma$  entering in the MHD equation for the bulk pressure), in order to neglect the coupling of Alfvén waves with the magneto-acoustic ones. For  $n=1$ , the most unstable mode, with dominant poloidal component  $m=2$ , is a Reversed Shear Alfvén Eigenmode (RSAE) driven by the energetic particles, (see Fig.3 where the simulation retaining only FOW effects is shown). The mode is localized in frequency at  $\omega/\omega_{A0} \approx 0.1085$  just below the lower Alfvén continuum, radially at  $0.1 \leq s \leq 0.6$ , close to the location of the minimum  $q$ -profile and with a normalized growth-rate  $\gamma/\omega_{A0} \approx 0.028$ . Results related to the same case but retaining FLR and magnetic compression effects are qualitatively very similar to the previous one, with only small differences, in particular, for the growth-rate and frequency (see Fig.5).

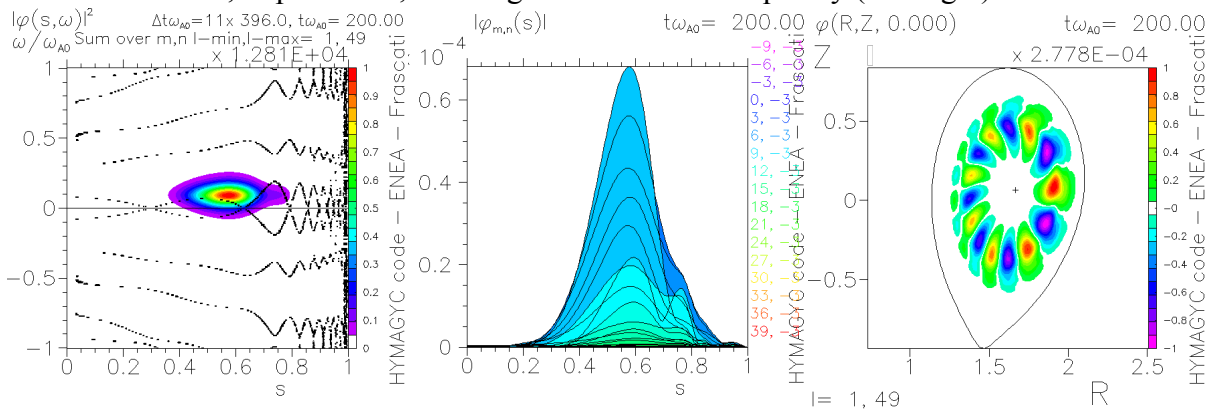


Fig.4. Toroidal mode number  $n=3$  retaining only FOW effects (same quantities as in Fig.3).

For  $n=3$ , a Toroidal Alfvén Eigenmode (TAE) is observed as the most unstable one, with dominant poloidal component  $m=7$  and a much richer Fourier spectrum (see Fig.4 where the results without FLR and magnetic compression effects, are shown). The mode is localized in frequency at  $\omega/\omega_{A0} \approx 0.0863$  just above the lower Alfvén continuum of the toroidal gap, and

radially, at  $0.4 \leq s \leq 0.8$ , with its peak located at the position of the maximum of the energetic particle pressure gradient. Its normalized growth-rate is  $\gamma/\omega_{A0} \approx 0.12472$ .

Also for this case, the results obtained retaining FLR and compressional effects are qualitatively similar to those of Fig.4, apart from a more pronounced reduction of the growth-rate, w.r.t. the  $n=1$  case. In Fig.5, the growth-rates and frequencies are shown vs.  $T_H$  for  $n=1$

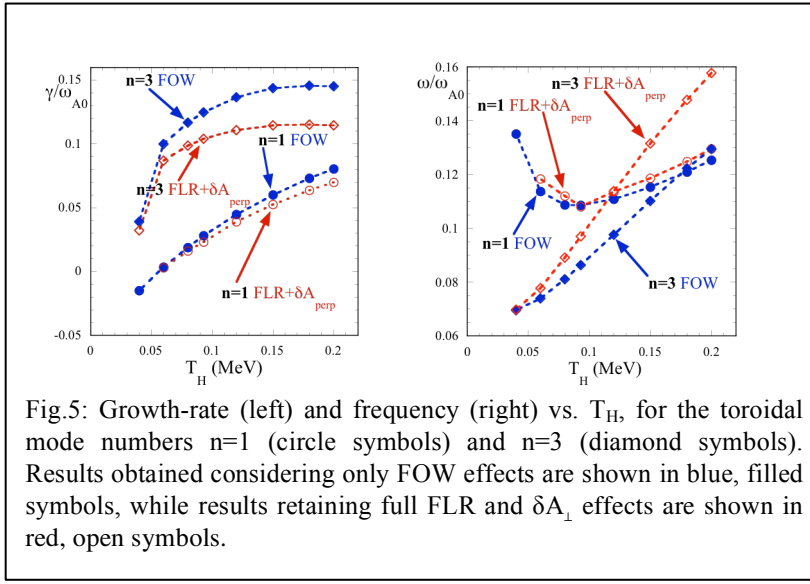


Fig.5: Growth-rate (left) and frequency (right) vs.  $T_H$ , for the toroidal mode numbers  $n=1$  (circle symbols) and  $n=3$  (diamond symbols). Results obtained considering only FOW effects are shown in blue, filled symbols, while results retaining full FLR and  $\delta A_\perp$  effects are shown in red, open symbols.

and  $n=3$ , both retaining and not retaining the FLR and compressional effects ( $\delta A_\perp \neq 0$ ). From Fig.5, left it is possible to observe how the FLR effects contribute to decreasing the growth-rate, as expected from earlier research [8] and [9]. The effect is stronger when the toroidal mode

number is higher (higher toroidal mode number implying larger  $k_\perp \rho_H$ ). Note that both CHEASE and MARS are already fully compliant with IMAS/EU-IM frameworks, while HYMAGYC is currently updating to the most up-to-date framework versions.

#### Acknowledgments

This work has been carried out within the framework of the EUROfusion Consortium and has received funding from the Euratom research and training programme 2014-2018 and 2019-2020 under grant agreement No 633053. The views and opinions expressed hereinto not necessarily reflect those of the European Commission. Part of the computing resources and the related technical support used for this work has been provided in part by the CRESCO/ENEAGRID High Performance Computing infrastructure and its staff [10].

#### References

- [1] G. Fogaccia, G. Vlad, S. Briguglio, Nucl. Fusion 56 (2016) 112004
- [2] Bondeson A., Vlad G. and Lütjens H. 1992 IAEA Technical Committee Meeting on Advances in Simulations and Modelling of Thermonuclear Plasmas (Montreal, 15–17 June 1992) p. 306 (Vienna, Austria: International Atomic Energy Agency)
- [3] Brizard A.J. and Hahm T.S. 2007 Rev. Mod. Phys. 79 421–68
- [4] Park W. et al 1992 Phys. Fluids B 4 2033
- [5] Ph.Lauber et al., NLED-AUG reference case, [http://www2.ipp.mpg.de/~pwl/NLED\\_AUG/data.html](http://www2.ipp.mpg.de/~pwl/NLED_AUG/data.html)
- [6] NLED Enabling Research Project, <https://www2.euro-fusion.org/erwiki/index.php?title=ER15-ENE-03>
- [7] Lütjens H., Bondeson A. and Sauter O. 1996 Comput. Phys. Commun. 97 219–60
- [8] N. N Gorelenkov, C. Z. Cheng, and G. Y. Fu Phys. Plasmas, 1999 Vol. 6, No.7
- [9] A. Könies et al 2018 Nucl. Fusion 58 126027
- [10] Ponti G. et al 2014 Proc. of the 2014 Int. Conf. on High Performance Computing and Simulation (Bologna, Italy, 21–25 July 2014) art. no. 6903807, pp 1030–3  
<http://ieeexplore.ieee.org/xpl/articleDetails.jsp?arnumber=6903807>